

# Commissioning of the ERDA-TOF beamline at the ion beam laboratory in Madrid

Andrés Redondo-Cubero<sup>a,b,\*</sup>, John A. Eliades<sup>c</sup>, Antonio Rodríguez<sup>a</sup>, David García-García<sup>b</sup>, Joonkon Kim<sup>a,c</sup>

<sup>a</sup> Centro de Micro-Análisis de Materiales, Universidad Autónoma de Madrid, 28049 Madrid, Spain

<sup>b</sup> Departamento de Física Aplicada, Universidad Autónoma de Madrid, 28049 Madrid, Spain

<sup>c</sup> Advanced Analysis Center, KIST, 5 Hwarang-ro 14-gil, Seoul 02792, Republic of Korea

## ARTICLE INFO

### Keywords:

ERDA  
TOF  
Telescope  
Resolution  
Efficiency  
IBA

## ABSTRACT

We report progress for the ERDA time-of-flight beamline at the Centre of Micro-Analysis of Materials in Madrid. This beamline experienced a long shut down and has recently gone through a re-commissioning process. The time stations, based on a twin mirror design, demonstrate a time resolution of 215 ps for 6 MeV He<sup>2+</sup>. Using a standard particle detector for the energy signal we find a mass resolution of 1.4 atomic mass units for <sup>27</sup>Al and <sup>28</sup>Si with 40 MeV Cl<sup>4+</sup>. Detection efficiency needs no corrections for elements heavier than <sup>7</sup>Li. Analysis of a borosilicate reference showed good agreement with the known composition. Based on these results, the facility is considered operational and open for users.

## 1. Introduction

Light elements play an important role in the development of technological materials since they can act as active impurities. Indeed, the presence of H, C, or O can strongly affect the operation of many nano-devices, being one of the main concerns when optimizing the growth of thin films and, particularly, of semiconductors. However, the detection of these elements is often challenging for many ion beam analysis (IBA) techniques, such as Rutherford backscattering spectrometry and particle induced X-ray emission [1]. In this sense, elastic recoil detection analysis (ERDA) performed with a time-of-flight and energy (TOF-E) spectrometer is a powerful approach to overcome the limitations [2,3], providing absolute quantification with isotope identification.

Several facilities have developed ERDA-TOF systems across Europe [4–10], America [11,12], Asia [13–15], Australia [16,17], and Africa [18]. Together with this progress, the analytical tools for ERDA-TOF have also become available for the scientific community, with reliable codes such as Potku [19] or Corteo [20] available for raw data analysis.

Despite these advances, some ion beam laboratories still lack instrumentation and know-how for this technique, as was the case in the Iberian Peninsula until now. An ERDA-TOF beamline was originally designed in 2004 at Centre of Micro-Analysis of Materials (CMAM) in Madrid (Spain) [21], but it experienced a series of problems that

prevented full operation and, therefore, experimental activity was restricted for some time [22–25]. In this work, we report the recent commissioning of the ERDA-TOF beamline at CMAM, where an extensive characterization has been carried out to determine the resolution, efficiency, and overall performance of the TOF telescope.

## 2. Experimental

### 2.1. Facility and beamline

CMAM is equipped with a 5 MV tandem accelerator from HVEE [26], and the ERDA-TOF beamline is located at the  $-10^\circ$  port of the switching magnet to allow the bending of the heavy ions. The total length from the switching magnet to the sample surface is 7.50 m. The beam spot is defined by two sets of collimating slits separated by 4.56 m. Beam current is measured with a Faraday cup placed before the scattering chamber. The sample is mounted in a motorized 3-axis goniometer (Arun Microelectronics).

Fig. 1 shows the design of the scattering chamber and the TOF-E telescope, placed at a  $40^\circ$  scattering angle. The length of flight between the time stations is 457 mm, and the total distance from the sample to the energy detector is 807 mm. A 4 mm circular collimator is placed before the telescope, which helps to reduce the count rate at the

\* Corresponding author at: Departamento de Física Aplicada, Universidad Autónoma de Madrid, 28049 Madrid, Spain.

E-mail address: [andres.redondo@uam.es](mailto:andres.redondo@uam.es) (A. Redondo-Cubero).

start station and restrict the angular divergence. The particle detector is an ultra-thin B-implanted Si detector (Ortec BU-016–300-100 model) with a nominal resolution of 16 keV and an active area of 300 mm<sup>2</sup>. Considering these geometrical conditions, the resulting angular opening is  $\pm 0.7^\circ$  and the solid angle of the spectrometer is 0.461 msr.

## 2.2. Time of flight detector

The inset of Fig. 1 shows a 3D model of a time station, which is based on the twin-mirror design from the University of Jyväskylä [27]. Two stations are used as clock triggers: the T1 station starts the TOF clock and the T2 station stops it. As ions pass through a station, secondary electrons are emitted from the centrally located C-foil and focused onto the detector microchannel plates (MCPs) using mirror plate electrodes. The stations were designed for optimum efficiency using a pyramidal “*toblerone*” geometry, so that secondary electrons emitted from both sides of the C foil are collected using 39° mirrors. This is the main important difference in terms of design when compared with conventional 45° stations [28], since it affects the electron trajectories and transport inside the station as discussed later.

In our system, identical voltages are used for both stations and were chosen based on the pulse height distribution (PHD) of the MCPs as a function of applied voltage. The mirrors are fixed at  $-3600$  V and the C foils at  $-3117$  V, with the supporting *toblerone* frame set at ground potential (0 V). Two MCPs are used in a chevron stack [29], with the upper surface of the first MCP biased at  $-2151$  V, and the lower surface of the second MCP biased at  $-220$  V. In this way, the electron landing energy stays in the keV range, as this is the optimal detection energy for MCPs [29,30]. A thin spacer ring is used between the two MCPs but no additional voltage is applied. Both MCPs, provided by Photonis, have 12.5  $\mu\text{m}$  pore diameter, 13° tilt angle, and 1:40  $d/L$  ratio. The anode, consisting of a Ni disc, is grounded to the processing circuit through an 18 k $\Omega$  current limiting resistor for safety. The distance between the anode and the MCP is 1.5 mm.

Originally, 31  $\mu\text{g}/\text{cm}^2$  self-standing C foils were used in both stations,

placed on frames with 12 mm and 18 mm diameter for the first and second stations, respectively. However, as described below, the time and mass resolutions from these foils was found to be unsatisfactory due to straggling and scattering. Therefore, they were recently replaced by thinner C foils (from Arizona Carbon Foils) with a nominal thickness of 5  $\mu\text{g}/\text{cm}^2$  and 10  $\mu\text{g}/\text{cm}^2$  for the T1 and T2 stations, respectively. Results using these foils show significant improvement, as described below. However, because they were only recently installed, the data is somewhat incomplete. Unless otherwise stated, results are for the 31  $\mu\text{g}/\text{cm}^2$  self-standing C foils.

The electronics for coincidence detection is based on conventional nuclear instrumentation modules. Both start and stop signals are collected from the time stations using a 1 GHz pre-amplifier and timing discriminator (Ortec 9327) and then fed into a time-to-amplitude converter (Ortec 567). Optionally, the delay of the start signal can be obtained by means of a passive delay box with 50, 100 and 200 ns cables. The energy signal is sent to a pre-amp (Ortec 142), then to the amplifier (Ortec 572A), and finally digitalized in an ADC (FAST ComTec 7072) and recorded using a multi-parameter acquisition unit (MPA3 from FAST ComTec). The coincidence window is set to 4  $\mu\text{s}$  and the signals are analyzed with a 1 GHz digital oscilloscope (Yokogawa DL6104). Typical count rates are  $\sim 20$  kHz in the first station (T1),  $\sim 2$  kHz in the second station (T2), and  $\sim 1$  kHz in the energy detector.

## 2.3. Computer simulations of the time stations

In order to test and better understand the characteristics of the timing stations, computer simulations were carried out using SIMION [31]. Electrons were given a starting energy, angle, and position at the foil surface. Voltages applied to the focusing plates, C-foil and deceleration grid were as described above in Section 2.2. Typically,  $10^4$  electrons were flown for each test using a time step control (t-quality in SIMION jargon) of 100. Initial energies were between 1 eV and 10 keV, representing the maximum range of ejection energies expected, although the most relevant contribution is expected for low energy

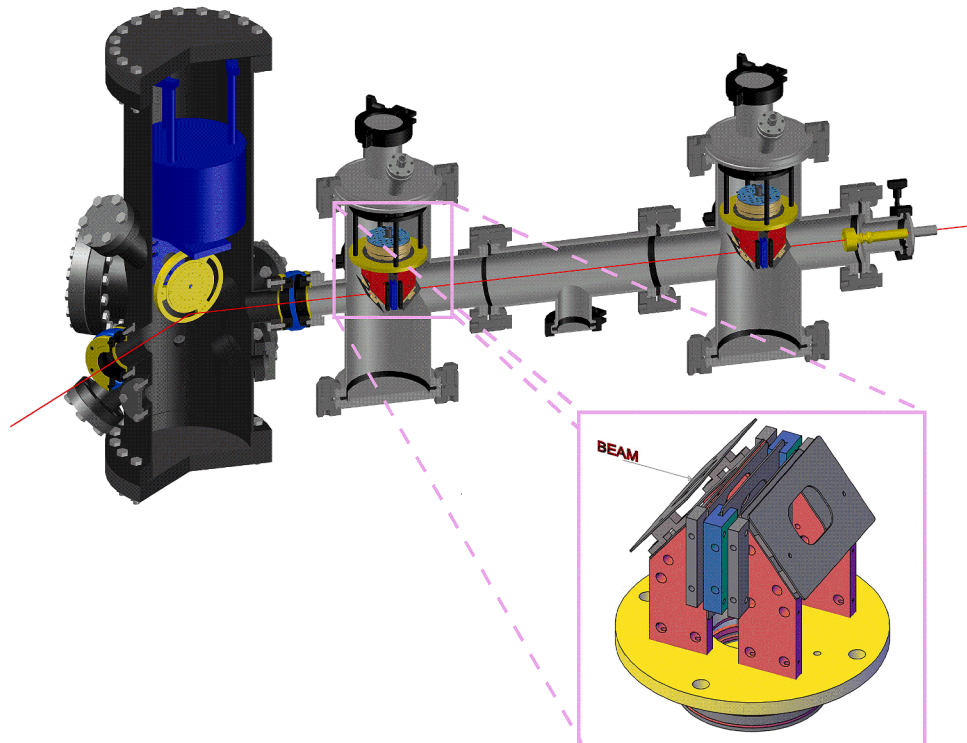


**Fig. 1.** 3D design of the scattering chamber and TOF-E telescope at CMAM. The length of flight between the stations is 457 mm and the total distance is 807 mm from the sample to the energy detector. Red line indicates the beam trajectory.

electrons (below 10 eV) [32]. To reproduce a more realistic ejection spread, electrons were started with a full-width angular distribution of  $\pm 40^\circ$ . Finally, ions were typically given a starting position within a filled disc of 10 mm diameter at the foil surface.

Fig. 2a shows two examples of simulations used to confirm the isochronous trajectories of the electrons. On the left side, 100 electrons with an initial energy of 1 eV are simulated (black lines) while, on the right side, electrons starting with 100 eV energy (blue lines) are simulated, both with the  $\pm 40^\circ$  angular distribution. The time of flight for 1 eV electrons to reach the MCPs was calculated to be 2.78(4) ns.

Fig. 2b shows the time-of-flight results for electrons to reach the MCPs over the full 1 eV to 10 keV simulation range. It is seen that this time remains essentially constant for energies below 500 eV. For higher energies, double reflection starts to produce longer and more inclined trajectories, which are no longer isochronous. Fig. 2c shows the corresponding collection efficiency over the full energy range. This efficiency is higher than 80 % for low energy electrons (<100 eV), but progressively decreases with energy. For 1 keV this efficiency is below 40 %. This confirms that the design is very suitable to capture low energy electrons but has some limitations for focusing high speed electrons.

### 3. Results and discussion

#### 3.1. Timing signal and resolution

Fig. 3 shows the raw timing signals from the T1 and T2 stations in a scattering experiment conducted with 2 MeV  $H^+$  on a thick Au target. These signals are clean negative pulses without echoes, demonstrating good performance of the stations. While the peak amplitude ( $>40$  mV) and FWHM ( $\sim 1$  ns) compare well with other reports, there is a significant improvement in the noise level [4,6].

Two types of experiment were used to evaluate the time resolution of the telescope. First, we used O beam scattering at different energies (from 4 to 24 MeV) on a 2 nm gold layer grown on a Si substrate. The

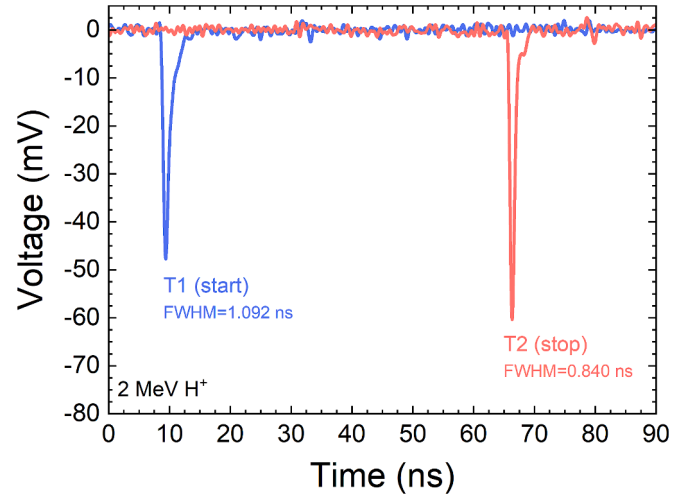


Fig. 3. Raw voltage signal (no amplification) from the time stations during a 2 MeV  $H^+$  scattering experiment on Au. FWHM of both peaks is close to 1 ns.

resolution for every energy was obtained from the FWHM of the O peak scattered from Au. For high energies, the extrinsic factors such as the energy spread and the flight length variations are minimized [33]. Fig. 4 shows the time resolution obtained, which had a stable value of 395(30) ps.

Second, we used the direct scattering of a 6 MeV  $He^{2+}$  beam on a thick gold sample (1  $\mu m$  Au layer on Si). The signal from the scattered beam was collected and the edge fit to an error function (inset in Fig. 4), with a resulting resolution of 435(12) ps. This value is in very good agreement with the intrinsic time resolution obtained for the O case.

While our resulting time resolutions are reasonably close to those obtained in other laboratories [6,9,13,33], especially if we take into account the significant straggling produced by the thick C foils used, we

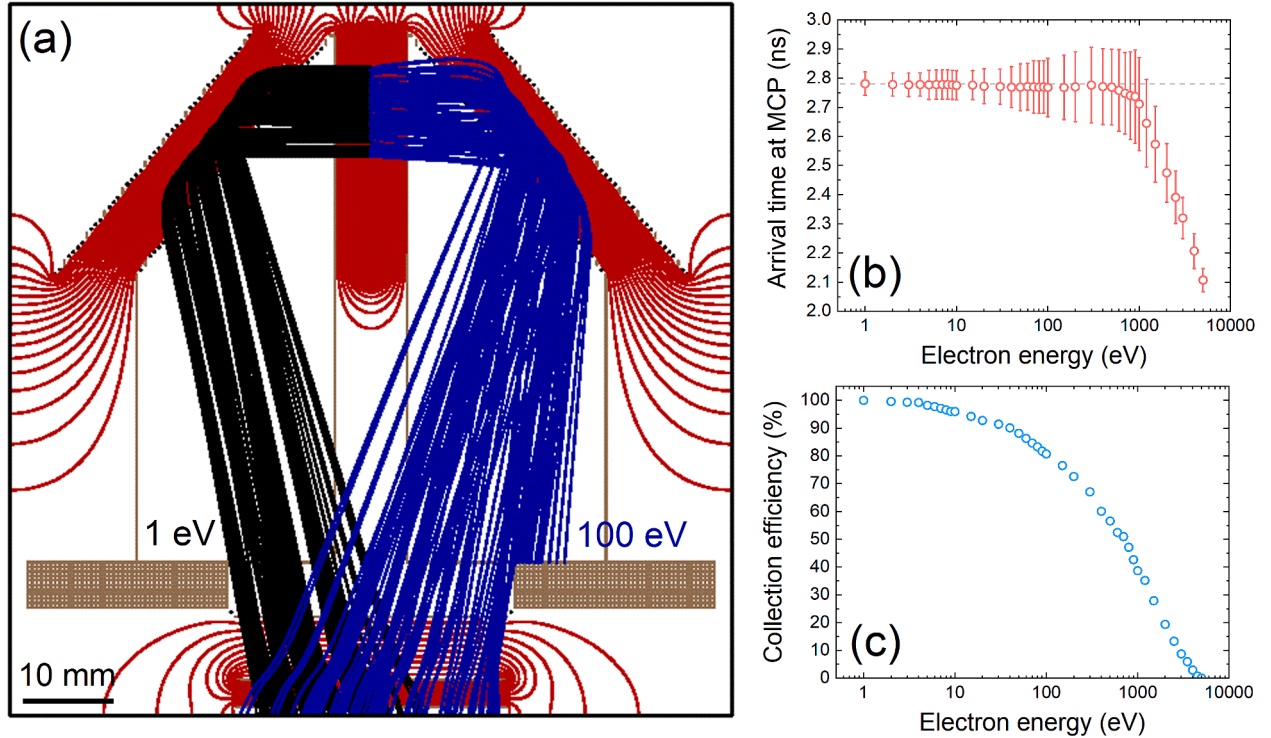
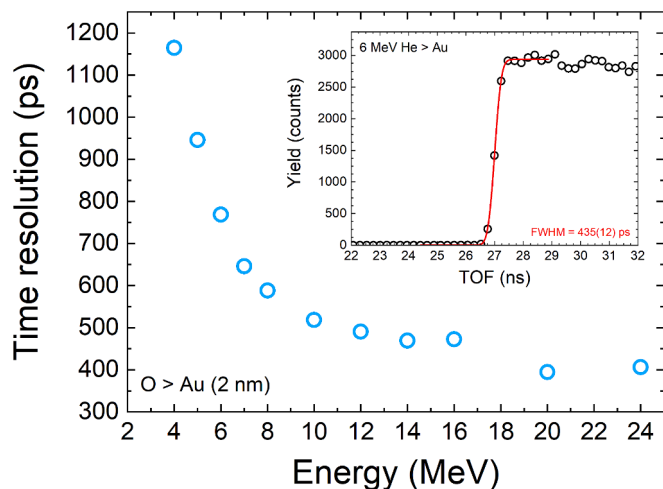


Fig. 2. (a) Simulations of electron trajectories with different starting energies inside the twin-mirror time station used at CMAM. On the left side (black lines), the initial energy of the electrons was 1 eV, while on the right side (blue lines) it was 100 eV. Red lines are equipotential lines with a 200 V step. (b) Electron arrival time at MCP for different initial energies. (c) Collection efficiency for different initial electron energies.



**Fig. 4.** Measurement of the time resolution using the scattering signal from O beam on 2 nm Au layer for different energies. The resolution saturates for high energies, with a final intrinsic value of 395(30) ps. Inset shows a comparison with 6 MeV  $\text{He}^{2+}$  scattering on a thick Au film, which leads to a similar time resolution of 435(12) ps.

felt that they could be improved. Therefore, we recently carried out experiments with a new set of thinner C foils ( $5 \mu\text{g}/\text{cm}^2$  at T1 and  $10 \mu\text{g}/\text{cm}^2$  at T2, section 2.2), obtaining a final resolution of 215(12) ps for 6 MeV  $\text{He}^{2+}$  scattered by thick Au. This is in line with state-of-the-art high resolution systems [4,7].

### 3.2. Mass resolution

The mass resolution is another important parameter that needs to be quantified. Light isotopes, such as  ${}^6\text{Li}/{}^7\text{Li}$ ,  ${}^{10}\text{B}/{}^{11}\text{B}$ , and  ${}^{12}\text{C}/{}^{13}\text{C}$ , were analyzed and shown to have complete separation in our spectrometer. The separation of  ${}^{27}\text{Al}$  and  ${}^{28}\text{Si}$  is typically more challenging and is used as a standard to evaluate mass resolution capabilities [7]. Thus, the mass resolution for a thin Al layer on a Si substrate was analyzed using recoil experiments at 20, 30 and 40 MeV  $\text{Cl}^{4+}$  impingement. The mass resolution for surface Al from Si was calculated to be 2.9, 1.8 and 1.4 atomic mass units (amu), respectively. Fig. 5 shows the spectrum for the representative case of 30 MeV, where partial overlapping of the signals

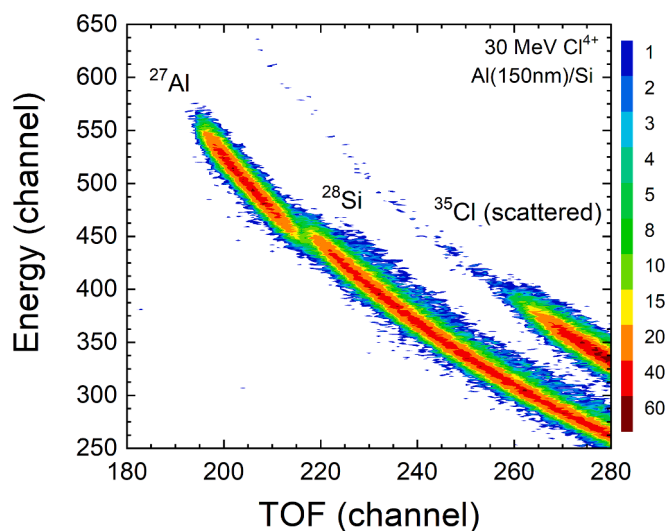


**Fig. 5.** ERDA-TOF spectra of a 150 nm Al layer on Si measured with 30 MeV  $\text{Cl}^{4+}$ . The  ${}^{27}\text{Al}$  and  ${}^{28}\text{Si}$  signals show partial overlapping, with a calculated mass resolution of 1.8 amu.

is visible, but the identification of the elements is still possible.

Straggling in the thick C foils and the reduced resolution of the particle detector are considered to be the major factors affecting our mass resolution. Therefore, it is reasonable to expect that mass resolution will improve considerably with installation of the new and thinner C foils, which showed improved time resolution over the thicker foils above. The characterization of this mass resolution will be carried out in future experiments.

### 3.3. Detection efficiency

The combined detection efficiency of the timing stations was tested for seven different ions:  ${}^1\text{H}$ ,  ${}^2\text{H}$ ,  ${}^4\text{He}$ ,  ${}^7\text{Li}$ ,  ${}^{11}\text{B}$ ,  ${}^{12}\text{C}$ , and  ${}^{16}\text{O}$ . For the experiments, the scattering events from a thick gold sample were recorded simultaneously both in coincidence ( $T1 \cdot T2 \cdot E$ ) and no coincidence (energy only). In the calculation we implicitly assume 100 % efficiency for the energy detector. The relative yields (triple coincidence vs. energy only) of the spectra were compared to obtain the efficiency at different energies, and the results are shown in Fig. 6.

It is well-known that H is the most challenging element to detect due to the low electron emission from C foils [34]. In our case, the efficiency for H is  $\sim 30\%$  for low energies (500 keV) and  $\sim 10\%$  for high energies (2 MeV). Although this latter value lies within the reported ranges by other laboratories [4,6,7], the efficiency for low energies is considerably lower.

There are several possible reasons for the drop in H detection efficiency at low energies. In order to explore some of these, we performed experiments with thin C foils ( $5 \mu\text{g}/\text{cm}^2$  and  $10 \mu\text{g}/\text{cm}^2$ ), obtaining small differences for the efficiency at low energies as compared to the thicker C foils. This indicates that secondary electron emission from the C foils is likely not the main limiting factor. We also verified that the MCPs were operating at the optimum gain, coinciding with 1 kV bias per MCP (below 850 V we observe a severe decrease in efficiency). However, the signal discrimination is limited by a threshold voltage, set to  $-10$  mV. This value cannot be reduced due to technical limitations of the discriminator, and, therefore, events producing small signals are not correctly processed. This might affect detection in a significant way when using light ions and, especially, H. This subject is still under investigation and will require further experiments to be completely clarified.

Efficiencies for  ${}^2\text{H}$ ,  ${}^4\text{He}$ , and  ${}^7\text{Li}$ , are  $\sim 20\%$ ,  $\sim 70\%$  and  $\sim 90\%$ , respectively, for 2 MeV ions. While these values reflect a smaller efficiency when compared to other spectrometers, they are better than the

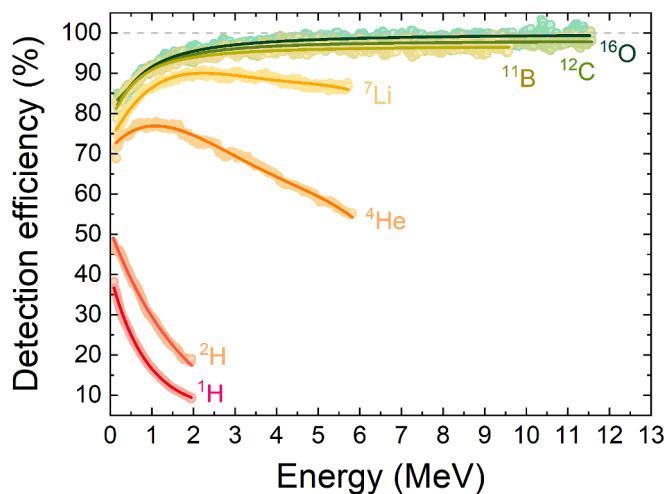


**Fig. 6.** Detection efficiency for different elements tested in scattering experiments on a gold target. Lines represent the best fits to the experimental values used for quantitative corrections during depth profile analysis.



results for  $^1\text{H}$ . No corrections are needed for elements heavier than  $^7\text{Li}$  according to our tests for  $^{11}\text{B}$ ,  $^{12}\text{C}$ , and  $^{16}\text{O}$  since detection efficiencies converge to unity for these ions above  $\sim 2$  MeV.

### 3.4. Test using borosilicate glass

In order to verify the overall performance of the telescope, we carried out an analysis of a borosilicate glass standard (Pyrex® Corning 7740). This type of glass has a nominal weight composition of 80.6 %  $\text{SiO}_2$ , 13.0 %  $\text{B}_2\text{O}_3$ , 4.1 %  $\text{Na}_2\text{O}$ , 2.3 %  $\text{Al}_2\text{O}_3$ , with trace constituents of  $\text{CaO}$ ,  $\text{MgO}$ ,  $\text{K}_2\text{O}$ , and other metal oxides [35–37]. Fig. 7a shows the spectrum of this sample analyzed with a 40 MeV  $\text{Au}^{7+}$  beam, where several elements can be identified, including a remarkable amount of H. The total acquisition time was 30 min.

Using Potku code [19], we calculated the corresponding depth profile which is shown in Fig. 7b. We found an atomic concentration of 61.8 % O, 30.8 % Si, 3.7 % H, 2.4 % B, 1.2 % Na and 0.09 % Ca respectively. These values are in good agreement with the nominal ones, which indicates that the quantification provides reliable values. The presence of Al and Mg could not be detected in the spectrum within the statistical error. However, the lack of these elements was also confirmed in an additional experiment carried out at the University of Jyväskylä with 11.9 MeV  $\text{Cu}^{6+}$ . Therefore, we can conclude that, if present in the sample, the atomic concentrations of these elements must be relatively low.

## 4. Conclusions

In this work we have described a newly installed TOF-E telescope at CMAM for high resolution ion beam analysis, evaluating the time and mass resolutions, and detection efficiency. The intrinsic time resolution was determined to be 395(30) ps when using a relatively thick set of 31  $\mu\text{g}/\text{cm}^2$  C foils for secondary electron emission, but was greatly improved to 212(12) ps resolution when using much thinner 5 and 10  $\mu\text{g}/\text{cm}^2$  C foils. The mass resolution for light isotopes was found to be inline with other laboratories. Using 40 MeV  $\text{Cl}^{4+}$ , separation of  $^{27}\text{Al}$  and  $^{28}\text{Si}$  was demonstrated to be up to 1.4 amu. While the detection efficiency of our system for light elements is relatively low, especially in the case of  $^1\text{H}$ , no corrections are needed for elements heavier than  $^7\text{Li}$  (as long as the energy is high enough). Finally, the practical performance of the spectrometer was tested using a standard reference borosilicate sample, finding good agreement with the known composition.

Based on these results, the ERDA-TOF beamline at CMAM has been deemed ready for operation, with routine beams of  $^{35}\text{Cl}$ ,  $^{79}\text{Br}$  or  $^{127}\text{I}$  ions using a typical energy of 20 MeV. Further improvements are expected soon, focused on the resolution and efficiency of the telescope with new time stations, thinner foils, and a new energy detector. This is, for the moment, the only facility of its kind in the Iberian Peninsula that will provide access to external users. This facility has potential applications in many emerging research projects and collaborations, such as the recent Chips for Europe Initiative or the Research Infrastructure Access in Nanoscience and Nanotechnology (RIANA).

### CRedit authorship contribution statement

**A. Redondo-Cubero:** Conceptualization, Methodology, Software, Validation, Formal analysis, Investigation, Resources, Data Curation, Writing - Original Draft, Writing - Review & Editing, Visualization, Supervision, Project administration, Funding acquisition. **John A. Eliades:** Conceptualization, Methodology, Software, Validation, Formal analysis, Investigation, Resources, Data Curation, Writing - Original Draft, Writing - Review & Editing, Visualization. **Antonio Rodríguez:** Software, Investigation, Visualization. **David García-García:** Investigation, Writing - Review & Editing. **Joonkon Kim:** Conceptualization, Methodology, Software, Validation, Formal analysis, Investigation, Resources, Data Curation, Writing - Original Draft, Writing - Review &

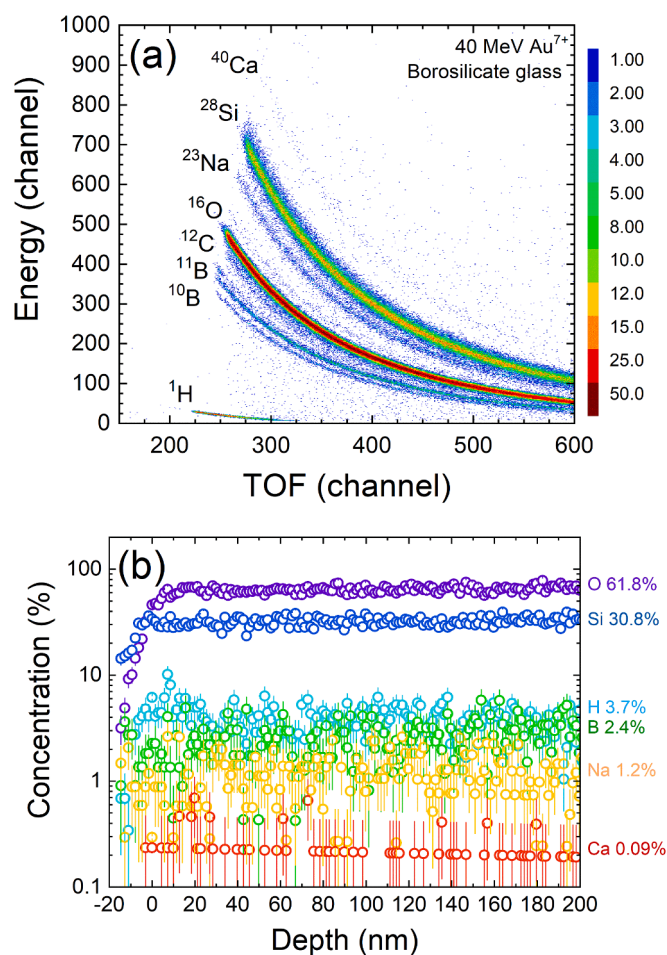


Fig. 7. (a) ERDA-TOF spectrum of a borosilicate glass (Pyrex®) measured with 40 MeV  $\text{Au}^{7+}$ . (b) Depth profile obtained with Potku software for the elements identified in the spectrum.

Editing, Visualization.

### Declaration of competing interest

The authors declare the following financial interests/personal relationships which may be considered as potential competing interests: Redondo-Cubero reports financial support was provided by Autonomous University of Madrid. The remaining authors declare that they have no known competing financial interests or personal relationships that could have appeared to influence the work reported in this paper.

### Acknowledgments

We are very grateful to the researchers from the University of Jyväskylä, for generously sharing their designs and know-how regarding the ERDA-TOF technique. We thank M. Laitinen, J. Julin, O. Beliuskina, and T. Sajavaara for valuable consulting, support, and training under the Guest Researcher Program under RADIATE project (EU Horizon 2020, grant 824096). We also thank fruitful discussions with K. Mizohata (University of Helsinki), F. Munnick (HZDR), Z. Siketić and I. Bogdanović (RBI), also possible through RADIATE Guest Researcher Program. We thank A. Muñoz for the long efforts constructing the beamline and the support from the technical team during all these years. Funding by MINECO project PID2021-127498NB-I00 is acknowledged.

## References

- [1] Y. Wang, M. Nastasi, Handbook Modern Ion Beam Materials Analysis, Materials Research Society, Warrendale, 2009.
- [2] J. L'Ecuyer, C. Brassard, C. Cardinal, J. Chabbal, L. Deschênes, J.P. Labrie, B. Terreault, J.G. Martel, R. St-Jacques, J. Appl. Phys. 47 (2008) 381–382.
- [3] R. Groleau, S.C. Gujrathi, J.P. Martin, Nucl. Instrum. Methods Phys. Res. B 218 (1983) 11–15.
- [4] M. Laitinen, M. Rossi, J. Julin, T. Sajavaara, Nucl. Instrum. Methods Phys. Res. B 337 (2014) 55–61.
- [5] J. Jokinen, J. Keinonen, P. Tikkanen, A. Kuronen, T. Ahlgren, K. Nordlund, Nucl. Instrum. Methods Phys. Res. B 119 (1996) 533–542.
- [6] S. Giangrandi, T. Sajavaara, B. Brijs, K. Arstila, A. Vantomme, W. Vandervorst, Nucl. Instrum. Methods Phys. Res. B 266 (2008) 5144–5150.
- [7] Z. Siketić, I.B. Radović, M. Jakšić, Nucl. Instrum. Methods Phys. Res. B 266 (2008) 1328–1332.
- [8] P. Ström, P. Petersson, M. Rubel, G. Possnert, Rev. Sci. Instrum. 87 (2016) 103303.
- [9] C. Kottler, M. Döbeli, F. Glaus, M. Suter, Nucl. Instrum. Methods Phys. Res. B 248 (2006) 155–162.
- [10] A. Razpet, P. Pelicon, Z. Rupnik, M. Budnar, Nucl. Instrum. Methods Phys. Res. B 201 (2003) 535–542.
- [11] M. Chicoine, F. Schiettekatte, M.I. Laitinen, T. Sajavaara, Nucl. Instrum. Methods Phys. Res. B 406 (2017) 112–114.
- [12] C.L. Fontana, C.-H. Chen, M.L. Crespillo, J.T. Graham, H. Xue, Y. Zhang, W. J. Weber, Nucl. Instrum. Methods Phys. Res. B 366 (2016) 104–116.
- [13] J.K. Kim, Y.S. Kim, G.D. Kim, H.W. Choi, H.J. Woo, S.Y. Cho, C.N. Whang, Nucl. Instrum. Methods Phys. Res. B 140 (1998) 380–388.
- [14] W. Hong, S. Hayakawa, K. Maeda, S. Fukuda, M. Yanokura, M. Aratani, K. Kimura, Y. Gohshi, I. Tanihata, Nucl. Instrum. Methods Phys. Res. B 124 (1997) 95–99.
- [15] K. Yasuda, Y. Kajitori, M. Oishi, H. Nakamura, Y. Haruyama, M. Saito, K. Suzuki, R. Ishigami, S. Hibi, Nucl. Instrum. Methods Phys. Res. B 442 (2019) 53–58.
- [16] H. Timmers, R.G. Elliman, G.R. Palmer, T.R. Ophel, D.J. O'Connor, Nucl. Instrum. Methods Phys. Res. B 136–138 (1998) 611–615.
- [17] J.W. Martin, D.D. Cohen, N. Dytlewski, D.B. Garton, H.J. Whitlow, G.J. Russell, Nucl. Instrum. Methods Phys. Res. B 94 (1994) 277–290.
- [18] M. Msimanga, D. Wamwangi, C.M. Comrie, C.A. Pineda-Vargas, M. Nkosi, T. Hlatshwayo, Nucl. Instrum. Methods Phys. Res. B 296 (2013) 54–60.
- [19] K. Arstila, J. Julin, M.I. Laitinen, J. Aalto, T. Konu, S. Kärkkäinen, S. Rahkonen, M. Raunio, J. Itkonen, J.-P. Santanen, T. Tuovinen, T. Sajavaara, Nucl. Instrum. Methods Phys. Res. B 331 (2014) 34–41.
- [20] F. Schiettekatte, Nucl. Instrum. Methods Phys. Res. B 266 (2008) 1880–1885.
- [21] A. Redondo-Cubero, M.J.G. Borge, N. Gordillo, P.C. Gutiérrez, J. Olivares, R. Pérez Casero, M.D. Ynsa, Eur. Phys. J. Plus 136 (2021).
- [22] A. Ropero-Real, N. Gordillo, J.L. Pau, A. Redondo-Cubero, ACS Appl. Mater. Interfaces 13 (2021) 56655–56662.
- [23] M. Gómez-Castaño, J.L. Pau, A. Redondo-Cubero, CrystEngComm 20 (2018) 3666–3672.
- [24] M. Gómez-Castaño, A. Redondo-Cubero, L. Vázquez, J.L. Pau, ACS Appl. Mater. Interfaces 8 (2016) 29163–29168.
- [25] R. Escobar Galindo, N. Benito, D. Duda, G.G. Fuentes, N. Valle, P. Herrero, L. Vergara, V. Joco, O. Sanchez, A. Arranz, C. Palacio, J. Anal. At. Spectrom. 27 (2012) 390–400.
- [26] A. Gotttdang, D.J.W. Mous, R.G. Haitsma, Nucl. Instrum. Methods Phys. Res. B 190 (2002) 177–182.
- [27] W.H. Trzaska, V. Lyapin, T. Alanko, M. Mutterer, J. Räisänen, G. Tjuri, M. Wojdyr, Nucl. Instrum. Methods Phys. Res. B 195 (2002) 147–165.
- [28] H.J. Whitlow, P. Jeanneret, E. Guibert, L. Wang, M. Van Der Meer, Nucl. Instrum. Methods Phys. Res. B 450 (2019) 385–389.
- [29] J. Ladislav Wiza, Nucl. Instrum. Methods 162 (1979) 587–601.
- [30] R.R. Goruganthu, W.G. Wilson, Rev. Sci. Instrum. 55 (1984) 2030–2033.
- [31] D.A. Dahl, Int. J. Mass Spectrom. 200 (2000) 3–25.
- [32] C.G. Drexler, R.D. DuBois, Phys. Rev. A 53 (1996) 1630–1637.
- [33] K. Yasuda, C. Batchuluun, R. Ishigami, S. Hibi, Nucl. Instrum. Methods Phys. Res. B 268 (2010) 2023–2027.
- [34] Z. Siketić, I.B. Radović, M. Jakšić, Thin Solid Films 518 (2010) 2617–2622.
- [35] American Society for Testing Materials, Standard Specification for Glasses in Laboratory Apparatus, 1996.
- [36] M.M. Smedskjaer, R.E. Youngman, J.C. Mauro, Appl. Phys. A 116 (2014) 491–504.
- [37] J.C. Phillips, R. Kerner, J. Chem. Phys. 128 (2008) 174506.